THE JOURNAL OF PHYSICAL CHEMISTRY C

ARTICLE

pubs.acs.org/JPCC

Atomic Layer Deposition of Fe_2O_3 Using Ferrocene and Ozone

Alex B. F. Martinson,[*,†,‡] Michael J. DeVries,[‡,∥] Joseph A. Libera,[‡,§] Steven T. Christensen,[‡,§] Joseph T. Hupp,[†,‡,∥] Michael J. Pellin,[†,‡,∥] and Jeffrey W. Elam[*,‡,§]

[†]Materials Science Division, [‡]Argonne-Northwestern Solar Energy Research (Anser) Center, and [§]Energy Systems Division, Argonne National Laboratory, 9700 South Cass Avenue, Argonne, Illinois 60439, United States

[∥]Department of Chemistry, Northwestern University, 2145 Sheridan Road, Evanston, Illinois 60208, United States

ABSTRACT: Growing interest in Fe_2O_3 as a light harvesting layer in solar energy conversion devices stems from its unique combination of stability, nontoxicity, and exceptionally low material cost. Unfortunately, the known methods for conformally coating high aspect ratio structures with Fe_2O_3 leave a glaring gap in the technologically relevant temperature range of 170−350 °C. Here, we elucidate a self-limiting atomic layer deposition (ALD) process for the growth of hematite, α-Fe_2O_3, over a moderate temperature window using ferrocene and ozone. At 200 °C, the self-limiting growth of Fe_2O_3 is observed at rates up to 1.4 Å/cycle. Dense and robust thin films grown on both fused quartz and silicon exhibit the expected optical bandgap (2.1 eV). In situ mass spectrometric analysis reveals the evolution of two distinct cyclic reaction products during the layer-by-layer growth. The readily available and relatively high vapor pressure iron precursor is utilized to uniformly coat a high surface area template with aspect ratio ∼150.

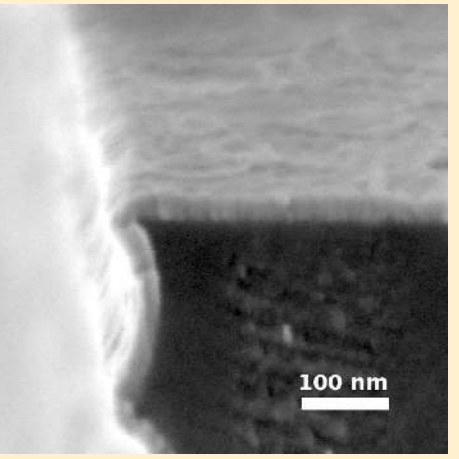

1. INTRODUCTION

Hematite (rhombohedral, α-Fe_2O_3) is the most common form of iron(III)oxide. An exceedingly stable substance, the familiar red polymorph is the principal constituent in rust. Hematite has been used throughout history in pottery and as a pigment and, more recently, has attracted attention for its electrical and optical properties. As a semiconductor, Fe_2O_3 is a potentially useful solar absorber and water oxidation catalyst.[1,2]

Growing interest in Fe_2O_3 as a light harvesting layer in solar energy conversion devices stems from its unique combination of stability, nontoxicity, and exceptionally low material cost. Although the 2.1 eV bandgap of hematite is not ideal for single-junction solar energy conversion devices, its potential in multijunction photovoltaics (PV) and photochemical conversion applications makes it an attractive target. The indirect bandgap material is a seemingly efficient light collector with peak absorptivity exceeding 10^5 cm^{-1}. Still, collecting 90% of incident photons with energy greater than the indirect gap would require a relatively thick film (∼1 μm). Given that the hole diffusion length within α-Fe_2O_3 is most often reported to be 2−20 nm,[3,4] utilizing a significant fraction of the incident solar flux will require alternative photoelectrode designs, ones that are characterized by both high surface areas and short charge−collection distances. Such designs will almost certainly entail nanoscale structuring.

By utilizing self-limiting surface reactions, atomic layer deposition (ALD) offers a general route to thin films that is uniquely suited to nanoscale structuring.[5] The technique is more appropriately classified as a surface-synthesis strategy comprising alternating chemical reactions that sequentially functionalize a substrate. Unlike other physical or chemical vapor deposition techniques, ALD employs self-limiting reactions that result in the growth of one atomic layer (or less) per A−B cycle. This elegant approach to material growth provides exquisite control over the thickness and composition of thin films. By its nature, ALD grows conformal films that have been shown to uniformly and reproducibly coat nanoscale architectures with aspect ratio in excess of 1000.[6,7] Several studies have shown the utility of ALD in the fabrication of nanostructured photovoltaics.[8−13] This study extends the range of high-aspect-ratio-compatible ALD processes suitable for the next generation of electro-optic devices.

The ALD of α-Fe_2O_3 was first demonstrated by alternating exposure to *tris*-(2,2,6,6-tetramethyl-3,5-heptanedionate)iron-(III) ($Fe(thd)_3$) and ozone (O_3).[14] While the self-limiting nature of the surface reaction was established, the process suffers from an exceptionally low growth rate (∼0.1 Å/cycle) and a small iron precursor vapor pressure, both of which limit its applicability to high aspect ratio coating. Subsequent reports of Fe_2O_3 formation via ALD include sequential substrate exposure to iron(III) *tert*-butoxide ($Fe_2(O^tBu)_6$) and water[15] as well as ferrocene ($Fe(Cp)_2$) pulsed alternately with molecular oxygen (O_2) at

Received: October 25, 2010
Revised: January 4, 2011
Published: February 22, 2011

high temperature.[16,17] While the $Fe_2(O^tBu)_6$ system has been shown to coat porous membranes with aspect ratio of 100, the narrow temperature window (130−170 °C) incites significant carbon incorporation. $Fe(Cp)_2$ has previously been used in combination with molecular oxygen at high temperatures (350−500 °C), but the self-limiting nature of the process remains unclear. A growth rate of 1.4 Å/cycle was reported for temperatures less than 500 °C, but differs substantially (0.6 Å/cycle) in porous membranes. Regardless, the known methods for conformally coating high aspect ratio structures with Fe_2O_3 leave a glaring gap in the technologically relevant temperature range of 170−350 °C. The ready application of a self-limiting, Fe_2O_3 ALD process utilizing commercially available, high vapor pressure precursors would stimulate the field.

In this Article, we describe a method for growing Fe_2O_3 by ALD using $Fe(Cp)_2$ and O_3. As compared to previous reports of ALD using $Fe(Cp)_2$ in combination with O_2, the use of O_3 enables growth over a much wider temperature range (100−250 °C). Furthermore, dense thin films that show only a single crystalline phase as grown are observed. Finally, the relatively large partial pressure of $Fe(Cp)_2$ (∼100 Pa at 80 °C) enables conformal deposition of Fe_2O_3 on high aspect ratio structures. While this is the first full report of ALD using these precursors, we note that one sentence was published during our studies that refers to ALD using $Fe(Cp)_2$ and O_3.[18] The authors report only the growth rate, 0.2 Å/cycle, one that differs markedly from those described herein.

2. EXPERIMENTAL SECTION

Fe_2O_3 ALD was performed using a viscous flow ALD reactor constructed of a stainless steel flow tube with an inside diameter of 5 cm to hold the substrates for film growth.[19] Ultrahigh purity (99.999%) nitrogen carrier gas continuously passed through the flow tube at a mass flow rate of 60 sccm and a pressure of 1.6 Torr. A constant reactor temperature was maintained by two temperature controllers connected to resistive heating elements attached to the outside of the reactor.

Fe_2O_3 ALD was performed using alternating exposures to $Fe(Cp)_2$ (Aldrich, >98%) and O_3 (∼10 wt % in 500 sccm ultrahigh purity O_2, Pacific Ozone). The $Fe(Cp)_2$ was held in a stainless steel bubbler maintained at 80 °C, while the tubing connecting the bubbler to the ALD reactor was maintained at 200 °C to prevent condensation of $Fe(Cp)_2$ on the reactor walls. The reaction tube and samples were heated to 200 or 250 °C as specified in the text. Ultrahigh purity nitrogen at a mass flow rate of 20 sccm was sent through the bubbler during $Fe(Cp)_2$ exposures and was diverted to bypass the bubbler following $Fe(Cp)_2$ exposures. Additional oxygen sources evaluated for Fe_2O_3 ALD included deionized water, hydrogen peroxide (Aldrich, 50 wt %), and O_2 (ultrahigh purity, 500 sccm). The ALD reactor was equipped with a quadrupole mass spectrometer (QMS, Stanford Research Systems RGA300) located downstream of the samples in a differentially pumped chamber separated from the reactor tube by a 35 μm orifice and evacuated using a 50 L/s turbomolecular pump.

The ALD timing sequences can be expressed as $t_1-t_2-t_3-t_4$, where t_1 is the exposure time for the first precursor, t_2 is the purge time following the first exposure, t_3 is the exposure time for the second precursor, t_4 is the purge time following the exposure to the second precursor, and all units are given in seconds (s).

The Fe_2O_3 films were deposited on Si(100) and fused quartz substrates. Prior to loading, the substrates were cleaned in an ultrasonicator using acetone and then isopropanol and blown dry using nitrogen. After loading, the substrates were allowed to outgas in the ALD reactor for 10 min at the deposition temperature in 1.6 Torr of flowing ultrahigh purity nitrogen. Next, the substrates were cleaned in situ using a 180 s exposure to O_3 in O_2 at a mass flow rate of 500 sccm.

Scanning electron microscopy (SEM) images were acquired using a Hitachi S4700 SEM with a field emission gun electron beam source, and an energy dispersive X-ray (EDX) detector for elemental analysis. X-ray diffraction (XRD) measurements were taken on a Rigaku Miniflex Plus diffractometer with Cu Kα radiation. Ellipsometric measurements of the Fe_2O_3 films deposited on Si(100) surfaces were performed using a J. A. Woolam Co. M2000 variable angle spectroscopic ellipsometer (VASE). Thin film thickness and density were also derived from fits to X-ray reflectivity (XRR) spectra acquired on a custom-built tool. The relative thickness of films grown on fused quartz was derived from X-ray fluorescence (XRF) measurements made using an Oxford Instruments ED2000. UV−vis−NIR reflection-corrected absorption spectra were derived from measurements employing a Varian Cary 5000 with integrating sphere accessory (DRA-2500). Silica aerogel films (∼9 μm thickness, aspect ratio 150) built on conductive glass platforms and micromachined Si trench wafers (aspect ratio 4) were coated with Fe_2O_3.

3. RESULTS AND DISCUSSION

Self-Limiting Growth Kinetics. The self-limiting nature of each half-cycle defines ALD as a surface-selective synthesis strategy and is paramount to the uniform coating of high aspect ratio structures. A true ALD process (with no CVD component) will exhibit saturating surface reactions such that in the limit of long precursor exposures a plateau in the growth rate is observed. Under our experimental conditions of constant precursor delivery in time, the exposure is strictly proportional to dose time. At 200 °C, both reactions are self-limiting and fit well to a Langmuir adsorption model, Figure 1.

The maximum growth rate in Figure 1a is limited by the selection of a subsaturating O_3 exposure, chosen in the interest of time. We note that this selection does not undermine the conclusion that can be drawn, that the $Fe(Cp)_2$ half-reaction is self-limiting at 200 °C. Under careful scrutiny, the growth rate dependence on ferrocene exposure reveals a mild slope in the long dose limit. Although many ALD precursors show "soft" saturation in the very high exposure limit,[20−22] the case of $Fe(Cp)_2$ in these studies is particularly intriguing due to the reported acceleration of $Fe(Cp)_2$ decomposition on vessels coated with Fe and C.[23] The result is an autocatalytic process in which the $Fe(Cp)_2$ decomposition products (containing Fe and C) stimulate the decomposition of $Fe(Cp)_2$ itself. The catalytic effect is so great that the kinetics of thermolysis have been measured at temperatures as low as 400 °C in Fe−C coated vessels.[23] This study is in discord with previous reports of ALD employing $Fe(Cp)_2$ and O_2 at 350−500 °C.[16,17] In published work examining the self-limiting nature of the $Fe(Cp)_2$ ALD surface reaction, reported only at 350 °C, the presence of a CVD component is unclear. Our experience with $Fe(Cp)_2$ at higher temperatures indicates that ALD growth at 250 °C is also practical although slightly less self-limiting. Fe_2O_3 ALD at temperatures above 300 °C using either O_2 or O_3 resulted in variable and sporadic growth rates and sometimes yielded visibly nonuniform, rough films. Other oxygen sources were explored under the

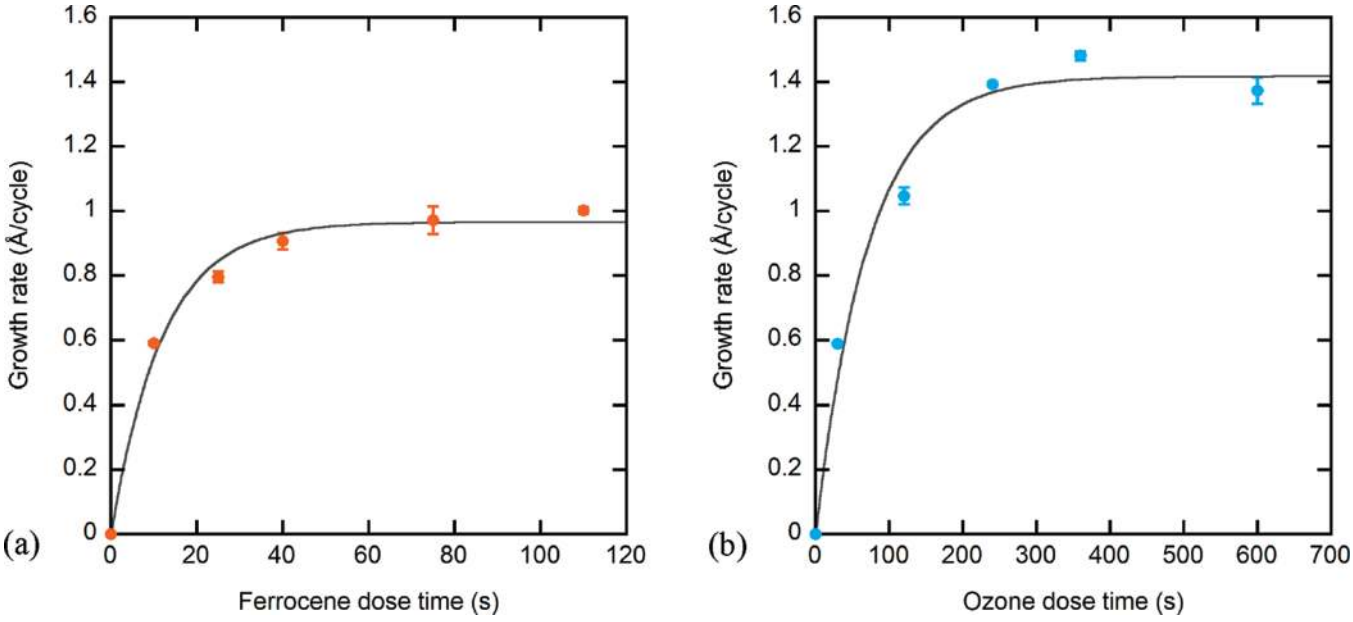

Figure 1. Fe_2O_3 growth rate at 200 °C versus the precursor dose time after 30 cycles of (a) $x-30-120-30$ where x is the $Fe(Cp)_2$ exposure time and (b) $40-30-y-30$ where y is the O_3 exposure time. The growth rate was determined from the average film thickness on samples located within 24 cm of the precursor inlet during a single run and is plotted with standard error. Solid lines are fits to a Langmuir adsorption model. The maximum growth rate in (a) is limited by the selection of a subsaturating O_3 exposure of 120 s.

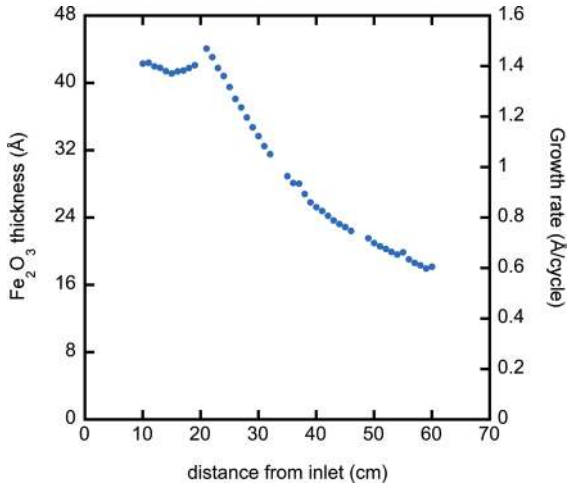

Figure 2. Fe_2O_3 growth rate at 200 °C as a function of distance from the multiport inlet at which precursors are introduced. Precursor dose timing is 40−30−240−30.

200 °C growth conditions. Alternating exposure to $Fe(Cp)_2$ and H_2O (60 s exposures) produces negligible growth. Attempts to deposit thin films using H_2O_2 (60 s) or pure O_2 (240 s) resulted in films of comparable quality, but depositions were slow and variable as compared to growth with O_3. Growth at temperatures as low as 100 °C using O_3 was also observed resulting in growth rates of ~0.3 Å/cycle but required very long purge times (90 s).

Under the standard ALD growth conditions at 200 °C, relatively large exposures of $\sim 10^7$ L (1 L = 1×10^{-6} Torr s) of both $Fe(Cp)_2$ and O_3 are required to reach saturated growth conditions on planar surfaces. These exposures are orders of magnitude greater than for typical ALD reactions, but are not without precedent. For example, reported ALD processes for SiN[24] and SiO_2[25] require $\sim 10^6$ and $>10^9$ L, respectively. For practical purposes, the vapor pressure of $Fe(Cp)_2$ may be increased by raising the precursor temperature, thereby reducing the length of the A cycle. A larger partial pressure of O_3, in contrast, may require quasi-static (stop-flow) operation or a higher initial O_3 concentration. With respect to photoelectrochemical applications, in which useful film thickness are typically less than 10 nm, the deposition rate (in time) is currently acceptable. Furthermore, for infiltrating nanoporous materials with very large aspect ratios, the infiltration kinetics can be diffusion limited[6] so that the unusually low reactivities of the $Fe(Cp)_2$ and O_3 are of little consequence.

Despite the self-limiting ALD process, film growth shows a reproducible dependence on the distance from the precursor inlet, Figure 2.

Although uncommon for ALD processes, a distance dependence on growth rate is not irreconcilable with self-limiting growth. Several growth mechanisms may explain this distance dependence. A first-order decomposition rate of one or both chemical precursors in the reactor tube will produce an exponentially decaying concentration gradient of precursor. The direct deposition of these decomposition products into thin films is one possibility, although it is inconsistent with the self-limiting nature of the half-reactions that were measured within 24 cm from the inlet, Figure 1. A second possibility is that the decomposition products are volatile, creating a quasi-steady state concentration profile of gas-phase precursors and decomposition products down the length of the reactor tube. Given the relative stability of ferrocene at these modest temperatures, metal precursor involvement in this mechanism is unlikely but cannot be excluded. In contrast, previous reports of the catalytic decomposition of O_3 over metal oxide surfaces, including Fe_2O_3, strongly support the possibility of an axial O_3 concentration gradient.[26] A third, more complex mechanism, in which decomposition products further inhibit or accelerate surface reaction kinetics, is also feasible. Water seems to be a possibility here, as relative humidity has been shown to alter the decomposition rate

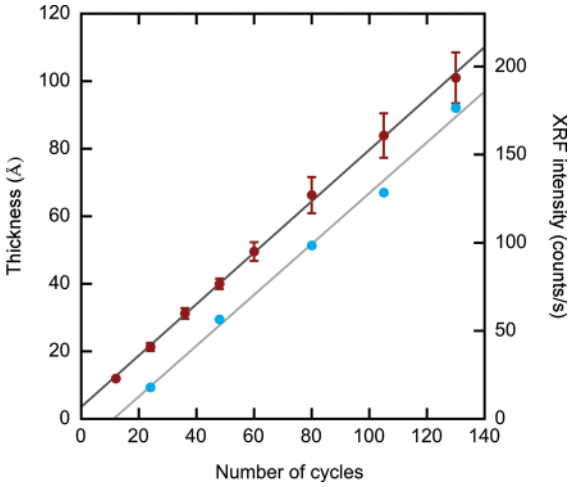

Figure 3. Fe_2O_3 film thickness on Si(100) (red ●) and XRF intensity on fused quartz (blue ●) versus number of $Fe(Cp)_2/O_3$ cycles at 200 °C using the timing 40−30−180−30. The average thicknesses of the two samples grown on Si(100) located closest to the precursor inlet are plotted with standard error. The solid lines are the best linear fit to the data.

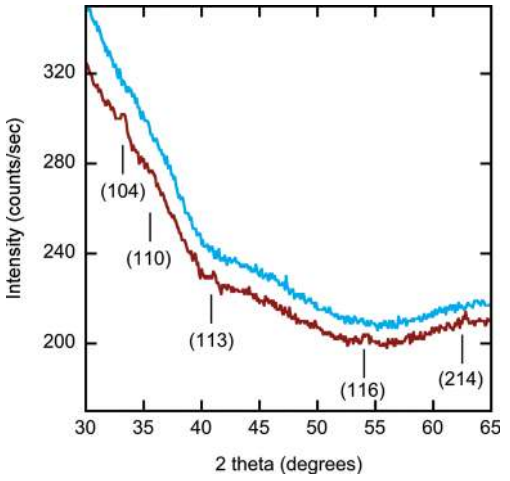

Figure 4. X-ray diffraction data from an 18 and 19 nm thick film grown on fused quartz at 200 °C (blue) and 250 °C (red), respectively. Peaks are referenced to α-Fe_2O_3 (PDF 00-033-0664). The nonzero baseline intensity is a result of the underlying fused quartz substrate.

Table 1. Growth Characteristics of Iron Oxide by ALD

iron precursor	O source	self-limiting growth temp (°C)	growth rate (Å/cycle)	reference
$Fe(thd)_3$	O_3	186	0.14	14
$Fe_2(O^tBu)_6$	H_2O	140	0.26	30
$Fe(Cp)_2$	O_2	350[a]	0.6−1.4	16
$Fe(Cp)_2$	O_3	200	1.4	herein

[a] Self-limiting behavior untested in the long-dose limit.

of O_3 over Fe_2O_3.[27] There is also evidence from mass spectroscopy studies (see below) that a slow evolution of reaction products occurs upon $Fe(Cp)_2$ dosing.

Surface Reaction Mechanism. In situ QMS measurements were employed to help elucidate the mechanism for Fe_2O_3 ALD using $Fe(Cp)_2$ and O_3. A survey of m/z ratios 1−200 revealed the primary products of the $Fe(Cp)_2$ reaction with the O_3-prepared surface to be m/z = 66 and 80, which (along with their characteristic mass cracks) are consistent with release of cyclopentadiene (HCp) and cyclopentadienone, respectively. HCp has been previously observed in similar metal−Cp ALD reactions, so its signature during the $Fe(Cp)_2$ reaction is not surprising.[28] The second reaction product, cyclopentadienone, is postulated on the basis of the slow and identical evolution of the following (in order of decreasing fraction): m/z = 80, 52, 26, 37, 51, 25, and 79. Cyclopentadienone is a feasible reaction product, although highly reactive[29] and previously unreported in ALD chemistry. During the O_3 reaction, m/z = 44 and 18 show the signature of combustion products and are evolved with a ratio of approximately 2:1, as may be expected from the burning of remaining surface-bound hydrocarbon-based ligands. Unfortunately, the slow reaction saturation kinetics combined with an inhomogeneous reactor coating (and therefore chemistry) prevent a more quantitative analysis of surface chemistry.

Thin-Film Growth. Robust, transparent thin films of Fe_2O_3 were grown homogeneously on both fused quartz and Si(100) between 100 and 250 °C. Excellent fits to ellipsometric spectra of all thickness were obtained by modeling a Cauchy dispersion layer over the wavelength range not absorbed by Fe_2O_3 (700−1000 nm). This method was further corroborated by comparison to thicknesses determined using literature values of the full spectrum (380−1000 nm) complex refractive index for Fe_2O_3 provided with the ellipsometric software. While excellent fits were obtained in the thin film limit, the full spectrum approach is less attractive due the changing imaginary component of the complex index of refraction as a function of film crystallinity (see absorptivity discussion below). Finally, X-ray reflectivity (XRR) was employed to infer the thickness, density, and roughness of a pair of films of thickness 7 and 13 nm. Agreement between XRR and ellipsometry derived thickness to within 3% was obtained for both films when the bulk density (5.27 g/cm^3) is best fit to 96% and 100% respectively. A roughness of 1−2 nm is derived from fits to XRR data for both films on fused quartz.

Linear growth was observed as a function of the number of ALD cycles on Si(100), Figure 3. On Si(100), there was no nucleation delay, as evidenced by the y-intercept crossing near the origin. Ellipsometry of the Fe_2O_3 films is problematic on fused quartz substrates due to reflection of the probe beam from the back of the substrate as well as the semitransparent nature of both substrate and thin film. To compare the growth rate on the different substrates, FeKα XRF was acquired for the fused quartz samples and compared to adjacent films on Si(100). When appropriately scaled, the XRF intensity produced a best fine line parallel to the thickness result on Si(100). The x-axis offset in relative thickness suggests a 16-cycle nucleation delay on fused quartz.

A summary of growth characteristics is presented in Table 1 where the $Fe(Cp)_2/O_3$ process is compared to previously reported iron oxide ALD processes.

The current ALD process exhibits a unique combination of moderate temperature and high growth rate. In addition, this Article describes the highest temperature ALD process shown to be self-limiting in the long-dose limit.

Properties of Fe_2O_3 Films. Iron oxide phase identification was performed using XRD. A component analysis of common iron oxide phases including hematite (α-Fe_2O_3), maghemite (γ-Fe_2O_3), magnetite (Fe_3O_4), and wustite (FeO) is feasible on the basis of the signature XRD patterns of each. In agreement with

dx.doi.org/10.1021/jp110203x |J. Phys. Chem. C 2011, 115, 4333–4339

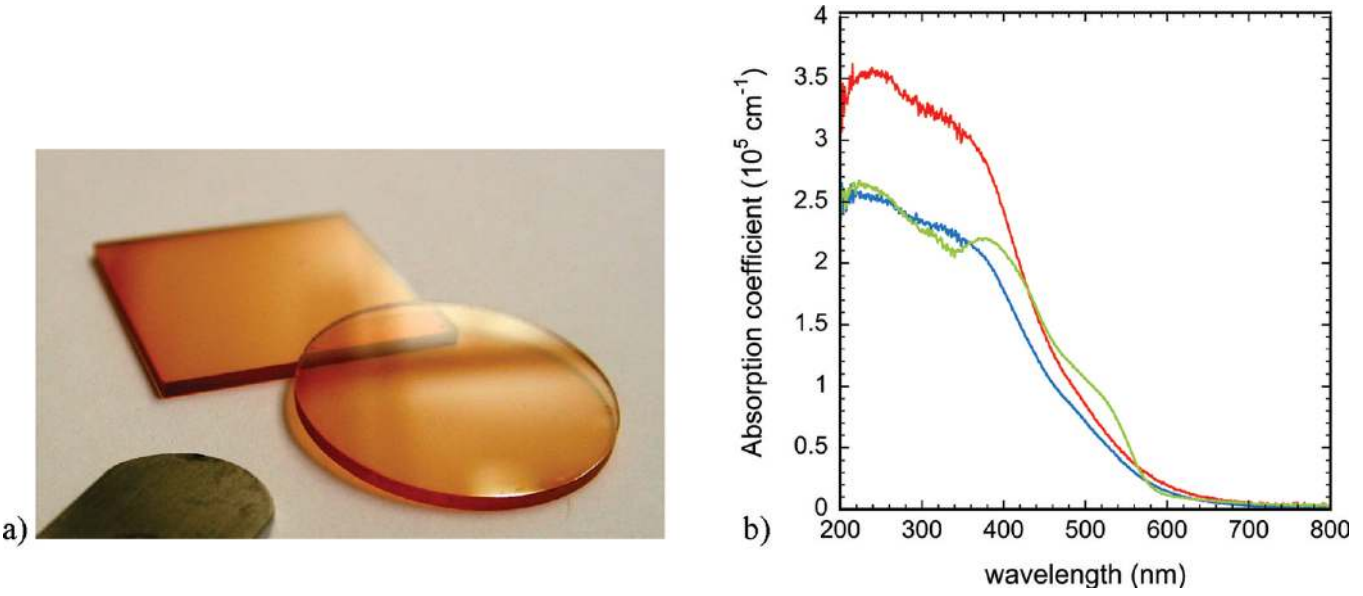

Figure 5. (a) Photograph of an 18 nm thick Fe_2O_3 film grown on fused quartz at 250 °C and (b) reflection-corrected absorption spectra of 6.7 nm (red), 12.6 nm (blue), and 15.3 nm (green) Fe_2O_3 thin films on fused quartz.

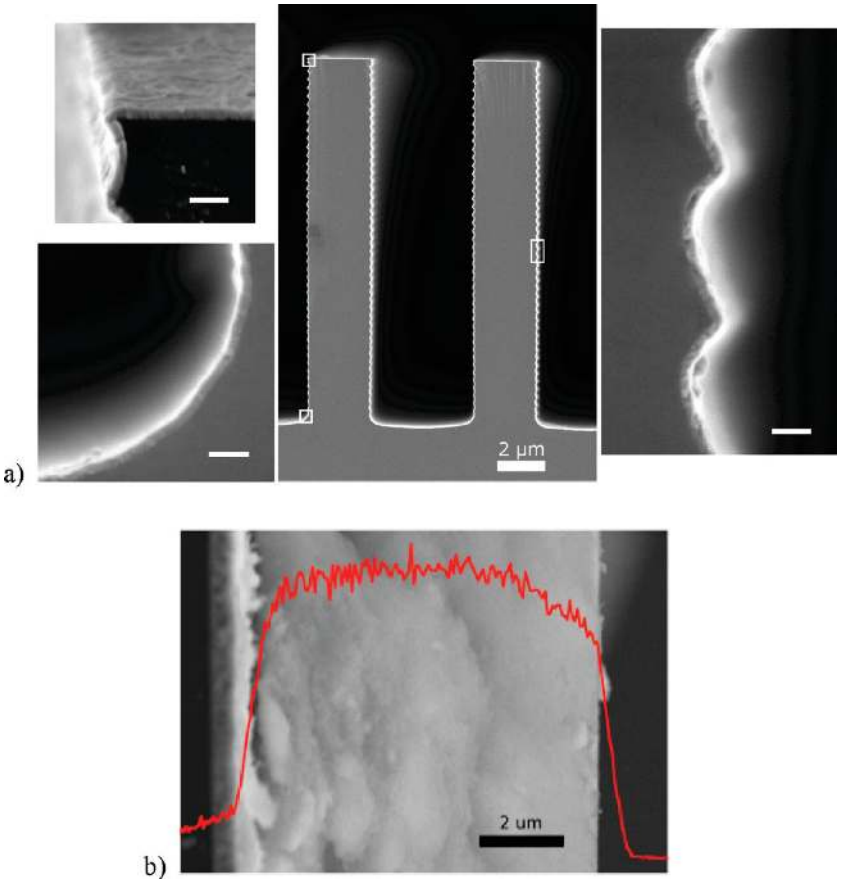

Figure 6. (a) SEM image of a conformal Fe_2O_3 thin film grown at 250 °C on a Si trench wafer. The scale bar on each of the three close-up images is 100 nm.(b) Cross-sectional SEM image of a 9 μm thick silica aerogel film coated with Fe_2O_3 by ALD and subsequently cleaved. The image is overlaid with Fe Kα intensity as measured by cross-sectional EDX (red line).

ellipsometric analysis, no crystallinity was detected by diffraction for films less than 14 nm. Above this thickness, XRD patterns that match rhombohedral, polycrystalline α-hematite (PDF 00-033-0664) were observed for films grown at 250 °C, Figure 4. The

dx.doi.org/10.1021/jp110203x |*J. Phys. Chem. C* 2011, 115, 4333–4339

Table 2. Physical Properties of Iron Oxide Grown by ALD

iron precursor	O source	crystalline phases observed	achieved aspect ratio	reference
$Fe(thd)_3$	O_3	α-Fe_2O_3	not reported	14,34
$Fe_2(O^tBu)_6$	H_2O	not reported	100	18,30
$Fe(Cp)_2$	O_2	mixed	30	16
$Fe(Cp)_2$	O_3	α-Fe_2O_3	>150	herein

lack of diffraction peaks in thin films grown at 200 °C suggests a predominantly amorphous material, although some crystalline character (not resolved by our XRD) is postulated on the basis of the evolution of structure in the complex index of refraction spectra as observed by ellipsometry.

In contrast to previous reports of Fe_2O_3 ALD by alternating $Fe(Cp)_2$ with molecular oxygen (O_2) at the self-limiting temperature,[16] films grown with O_3 are not of mixed phase. The strongly oxidizing oxygen source in the present system likely precludes the mixing of less oxidized forms of iron such as magnetite (Fe_3O_4). That the presence of O_3 induces higher oxidation states of iron is further supported by previous reports of ALD using $Fe(thd)_3$ with O_3 in which only hematite was observed.[14]

Quantitative compositional analysis of a thin film grown at 200 °C was performed using Rutherford backscattering spectroscopy (RBS) and the amount of H quantified by hydrogen forward scattering (HFS). The atomic ratio of the primary film constituents Fe:O is observed to be 1:0.61, which is consistent with a slightly oxygen-rich stoichiometry of $Fe_2O_{3.3}$. The primary impurity is hydrogen, which is present in 7 ± 1 atomic % and suggests the possibility of some iron(III) oxide−hydroxide incorporation, for example, FeO(OH). The remaining impurity in the film (<1 atomic %) is consistent with Nb, the major metal deposited on our shared ALD tool. Carbon appeared at the film surface but was not detected in the film (C detection limit of the method is 4 atomic %). Here again, the film quality appears to benefit from O_3, this time as a result of the probable oxidation of carbon-containing residues that may otherwise contaminate the films during the relatively low temperature growth.

The optically transparent and homogeneous thin films exhibited an intense red-orange "rust" color characteristic of hematite, Figure 5a. Reflection-corrected extinction spectra at several thin film thicknesses, Figure 5b, revealed strong and structured absorptivity out to approximately 600 nm (2.1 eV), in agreement with literature reports.[31−33]

The absorptivity was observed to decrease slightly, and several spectral features grew in as the film increased in thickness. At least four distinct spectral features are observed in the thickest film, while films less than 14 nm thickness showed similar but more subtle structure. The position of each peak (223, 315, 375, and 535 nm) is in excellent agreement with transitions calculated for hematite as well as those experimentally observed for polycrystalline thick films.[32] The absorptivity of the thickest film is also a close match to that recently reported for hematite thick films fired in air at 400 °C.[33] The lack of order in the thinner, amorphous films may relax the selection rules for photon absorption such that the amorphous semiconductor, which is indirect in its crystalline form, shows greater absorptivity. The extinction spectra support the prior assertion that the ultrathin Fe_2O_3 films are amorphous, with the hematite phase growing in significantly at 14 nm.

Growth on High-Aspect-Ratio Templates. The ability to coat high-aspect-ratio structures conformally demonstrates the potential of this process for use in photoelectrochemical applications in which great light harvesting is beneficial. Long dose times were used to grow thin hematite films on both Si trench wafers and thick-film silica aerogels. Scanning electron microscopy (SEM) and cross-sectional energy dispersive X-ray spectroscopy (EDX) were used to verify the conformality and penetration of iron oxide into the porous structures. A cross-section SEM of a cleaved Si trench wafer (aspect ratio 4) reveals a conformal thin film on all surfaces of the convoluted substrate, Figure 6a.

Oblique angle, high magnification images further corroborate ellipsometric and XRR evidence for smooth and dense films. A 9 μm thick porous silica framework was also coated by ALD and subsequently fractured for analysis. The cross-sectional EDX spectrum of Fe Kα overlaying the thick porous structure, Figure 6b, clearly illustrates the uniform and deeply penetrating coating characteristics using the $FeCp_2/O_3$ ALD process. As the largest pores in the aerogel are less than 60 nm, an aspect ratio greater than 150 is calculated.

A comparison of thin film properties produced by the $FeCp_2/O_3$ ALD process relative to those for previously reported iron oxide routes, Table 2, reveals several pertinent differences.

The exclusion of less oxidized forms of iron is pertinent for photoelectrochemical applications in particular. Indeed, air annealed Fe_2O_3 thin films grown by ALD using $Fe(Cp)_2$ and ozone have recently been utilized in regenerative photoelectrochemical cells.[35]

4. CONCLUSIONS

We have elucidated a self-limiting ALD process for the growth of hematite, α-Fe_2O_3, over a moderate temperature window using ferrocene and ozone. The system is likely to be particularly well suited to photoelectrochemical applications due to the unique convergence of ample ALD growth per cycle and resulting thin film quality. Alternating exposure to molecular precursors at 200 °C enables deposition of Fe_2O_3 films with a growth rate greater than 1 Å /cycle. The dense and robust films that result exhibit an optical bandgap of 2.1 eV and modest surface roughness. Uniformly coated high-aspect-ratio templates further demonstrate the self-saturating nature of each reaction and suggest the possibility of further utility in the future.

AUTHOR INFORMATION

Corresponding Author

*E-mail: martinson@anl.gov (A.B.F.M.), jelam@anl.gov (J.W.E.).

ACKNOWLEDGMENT

This work was supported as part of the Argonne-Northwestern Solar Energy Research (ANSER) Center, an Energy Frontier Research Center funded by the U.S. Department of Energy, Office of Science, Office of Basic Energy Sciences, under Award Number DE-SC0001059. The electron microscopy was performed at the Electron Microscopy Center for Materials Research (EMCMR) at Argonne National Laboratory. Use of the EMCMR was supported by the U.S. Department of Energy, Office of Science, Office of Basic Energy Sciences, under Contract No. DE-AC02-06CH11357 operated by UChicago Argonne, LLC. We thank Vennesa Williams for fabrication of the porous aerogel thick film.

REFERENCES

(1) Kennedy, J. H.; Frese, K. W. J. *J. Electrochem. Soc.* **1978**, *125*, 709.
(2) Kay, A.; Cesar, I.; Gratzel, M. *J. Am. Chem. Soc.* **2006**, *128*, 15714.
(3) Kennedy, J. H.; Frese, K. W., Jr. *J. Electrochem. Soc.* **1978**, *125*, 709.
(4) Dare-Edwards, M. P.; Goodenough, J. B.; Hamnett, A.; Trevellick, P. R. *J. Chem. Soc., Faraday Trans. 1* **1983**, *79*, 2027.
(5) Ritala, M.; Leskela, M. In *Handbook of Thin Film Materials*; Nalwa, H. S., Ed.; Academic Press: San Diego, 2001; Vol. 1, p 103.
(6) Elam, J. W.; Routkevitch, D.; Mardilovich, P. P.; George, S. M. *Chem. Mater.* **2003**, *15*, 3507.
(7) Biener, J.; Baumann, T. F.; Wang, Y. M.; Nelson, E. J.; Kucheyev, S. O.; Hamza, A. V.; Kemell, M.; Ritala, M.; Leskela, M. *Nanotechnology* **2007**, *18*, 055303.
(8) Nanu, M.; Schoonman, J.; Goossens, A. *Adv. Mater.* **2004**, *16*, 453.
(9) Law, M.; Greene, L. E.; Radenovic, A.; Kuykendall, T.; Liphardt, J.; Yang, P. D. *J. Phys. Chem. B* **2006**, *110*, 22652.
(10) Martinson, A. B. F.; Elam, J. W.; Hupp, J. T.; Pellin, M. J. *Nano Lett.* **2007**, *7*, 2183.
(11) Hamann, T. W.; Martinson, A. B. E.; Elam, J. W.; Pellin, M. J.; Hupp, J. T. *Adv. Mater.* **2008**, *20*, 1560.
(12) Hamann, T. W.; Martinson, A. B. F.; Elam, J. W.; Pellin, M. J.; Hupp, J. T. *J. Phys. Chem. C* **2008**, *112*, 10303.
(13) Martinson, A. B. F.; Elam, J. W.; Liu, J.; Pellin, M. J.; Marks, T. J.; Hupp, J. T. *Nano Lett.* **2008**, *8*, 2862.
(14) Lie, M.; Fjellvag, H.; Kjekshus, A. *Thin Solid Films* **2005**, *488*, 74.
(15) Bachmann, J.; Jing, J.; Knez, M.; Barth, S.; Shen, H.; Mathur, S.; Gosele, U.; Nielsch, K. *J. Am. Chem. Soc.* **2007**, *129*, 9554.
(16) Rooth, M.; Johansson, A.; Kukli, K.; Aarik, J.; Boman, M.; Harsta, A. *Chem. Vap. Deposition* **2008**, *14*, 67.
(17) Scheffe, J. R.; Frances, A.; King, D. M.; Liang, X.; Branch, B. A.; Cavanagh, A. S.; George, S. M.; Weimer, A. W. *Thin Solid Films* **2009**, *517*, 1874.
(18) Escrig, J.; Bachmann, J.; Jing, J.; Daub, M.; Altbir, D.; Nielsch, K. *Phys. Rev. B* **2008**, *77*, 214421.
(19) Elam, J. W.; Groner, M. D.; George, S. M. *Rev. Sci. Instrum.* **2002**, *73*, 2981.
(20) Elam, J. W.; Baker, D. A.; Hryn, A. J.; Martinson, A. B. F.; Pellin, M. J.; Hupp, J. T. *J. Vac. Sci. Technol., A* **2008**, *26*, 244.
(21) Musschoot, J.; Xie, Q.; Deduytsche, D.; Van den Berghe, S.; Van Meirhaeghe, R. L.; Detavernier, C. *Microelectron. Eng.* **2009**, *86*, 72.
(22) Wind, R. A.; George, S. M. *J. Phys. Chem. A* **2010**, *114*, 1281.
(23) Dyagileva, L. M.; Mar'in, V. P.; Tsyganova, E. I.; Razuvaev, G. A. *J. Organomet. Chem.* **1979**, *175*, 63.
(24) Goto, H.; Shibahara, K.; Yokoyama, S. *Appl. Phys. Lett.* **1996**, *68*, 3257.
(25) Ferguson, J. D.; Weimer, A. W.; George, S. M. *Chem. Mater.* **2000**, *12*, 3472.
(26) Dhandapani, B.; Oyama, S. T. *Appl. Catal., B* **1997**, *11*, 129.
(27) Mogili, P. K.; Kleiber, P. D.; Young, M. A.; Grassian, V. H. *J. Phys. Chem. A* **2006**, *110*, 13799.
(28) Elam, J. W.; Baker, D. A.; Martinson, A. B. F.; Pellin, M. J.; Hupp, J. T. *J. Phys. Chem. C* **2008**, *112*, 1938.
(29) Harmata, M.; Barnes, C. L.; Brackley, J.; Bohnert, G.; Kirchhoefer, P.; Kurti, L.; Rashatasakhon, P. *J. Org. Chem.* **2001**, *66*, 5232.
(30) Bachmann, J.; Jing, J.; Knez, M.; Barth, S.; Shen, H.; Mathur, S.; Gosele, U.; Nielsch, K. *J. Am. Chem. Soc.* **2007**, *129*, 9554.
(31) Dare-Edwards, M. P.; Goodenough, J. B.; Hamnett, A.; Trevellick, P. R. *J. Chem. Soc., Faraday Trans. 1* **1983**, *79*, 2027.
(32) Marusak, L. A.; Messier, R.; White, W. B. *J. Phys. Chem. Solids* **1980**, *41*, 981.
(33) Sivula, K.; Zboril, R.; Le Formal, F.; Robert, R.; Weidenkaff, A.; Tucek, J.; Frydrych, J.; Gratzel, M. *J. Am. Chem. Soc.* **2010**, *132*, 7436.
(34) Nilsen, O.; Lie, M.; Foss, S.; Fjellvag, H.; Kjekshus, A. *Appl. Surf. Sci.* **2004**, *227*, 40.
(35) Klahr, B. M.; Martinson, A. B. F.; Hamann, T. W. *Langmuir* **2010**, *27*, 461.